For submission to Tissue Engineering: Part A

Decellularised cartilage directs chondrogenic differentiation: creation of a fracture callus mimetic

Wollis J. Vas[1], Mittal Shah[1], Thomas S. Blacker[2, 3], Michael R. Duchen[2], Paul Sibbons[4] and Scott J. Roberts[1].

[1] Department of Materials and Tissue, Institute of Orthopaedics and Musculoskeletal Science, University College London, Stanmore, UK.

[2] Department of Cell and Developmental Biology, University College London, London UK.

[3] Department of Physics and Astronomy, University College London, London UK.

[4] Northwick Park Institute for Medical Research, Northwick Park Hospital, London, UK

*Corresponding Author: Dr Scott Roberts

Department of Materials and Tissue, Institute of Orthopaedics and Musculoskeletal Science, University College London, Stanmore, UK.

scott.roberts@ucl.ac.uk

Keywords

Bone tissue engineering; Periosteal stem cells; Non-union fractures; Chondrogenesis; Hypertrophic cartilage; Bone grafts; Bone regeneration

2

Abstract

Complications that arise from impaired fracture healing have considerable socioeconomic implications. Current research in the field of bone tissue engineering predominantly aims to mimic the mature bone tissue microenvironment. This approach, however, may produce implants that are intrinsically unresponsive to the cues present during the initiation of fracture repair. As such, this study describes the development of decellularised xenogeneic hyaline cartilage matrix in an attempt to mimic the initial reparative phase of fracture repair. Three approaches based on vacuum-assisted osmotic shock (Vac-OS), Triton X (Vac-Stx) and SDS (Vac-SDS) were investigated. The Vac-OS methodology reduced DNA content below 50ng/mg of tissue, whilst retaining 85% of the sGAG content and as such was selected as the optimal methodology for decellularisation. The resultant Vac-OS scaffolds (dcECM) were also devoid of the immunogenic alpha-gal epitope. Furthermore, minimal disruption to the structural integrity of the dcECM was demonstrated using differential scanning calorimetry (DSC) and fluorescence lifetime imaging microscopy (FLIM). The biological integrity of the dcECM was confirmed by its ability to drive the chondrogenic commitment and differentiation of human chondrocytes and periosteum-derived cells respectively. Furthermore, histological examination of dcECM constructs implanted in immunocompetent mice revealed a predominantly M2-macrophage driven regenerative response both at 2 and 8 weeks post-implantation. These findings contrasted with the implanted native costal cartilage that elicited a predominantly M1-macrophage mediated inflammatory response. This study highlights the capacity of dcECM from the Vac-OS methodology to direct the key biological processes of endochondral ossification, thus potentially recapitulating the callus phase of fracture repair.

1. Introduction

Bone tissue has a remarkable capacity for regeneration, driven by mechanisms that govern embryonic bone development [1]. Despite this, both internal and external pathological factors can hinder the fracture healing process, resulting in delayed or non-union fractures [2,3].

Autologous bone grafting (ABG) remains the current gold standard treatment approach but is hindered by major limitations such as tissue availability and donor site morbidity [4–6]. Tissue engineering strategies have attempted to produce alternatives, primarily through mimicking the desirable properties of ABG [7,8]. These approaches, however, mainly aim to mimic mature bone tissue and are therefore intrinsically unresponsive to the important biological cues present during early fracture repair. This has led to the investigation of endochondral ossification [9], which predominates during embryonic bone formation and is also a key driver of long bone fracture repair postnatally [2,3]. The cartilaginous callus formed during endochondral fracture repair produces factors that are known to promote angiogenesis and calcification, subsequently promoting matrix remodelling [10–12]. It has therefore been proposed that recapitulating endochondral ossification, or at least the tissue intermediates involved in this process, may facilitate bone healing more effectively [13–16].

Although there have been major advances in the fabrication of synthetic biomaterials, their limited ability to be remodelled during the complex process of tissue formation results in limited integration[17–21]. Therefore, the use of naturally derived ECM constructs is highly appealing as they should be susceptible to tissue remodelling processes. Indeed, much research has been associated with the use of decellularised tissues from other species to create biological scaffolds. Decellularised biological scaffolds not only retain the original 3D morphological architecture of the tissue but, with appropriate attention to production processes, can also retain a complex mixture of proteins and macromolecules that aid the proliferation and differentiation of endogenous or exogenous cells. Importantly, the structural and functional proteins of the ECM are highly conserved across species. This high degree of homology allows xenogeneic ECM to

4

be implanted in recipients of different species without an immune reaction [22]. The avoidance of tissue rejection in the recipient has catapulted the use of decellularised scaffolds to the forefront of regenerative medicine and tissue engineering, as evidenced by the success of human tracheal implants [23]. Additionally, a number of xenogenic bone void fillers are currently used clinically, such as NuOss™ (Ace Surgical) and Bio-Oss® (Geistlich), which are both derived from bovine bone tissue.

To date, most research incorporating naturally derived decellularised cartilage ECM for endochondral ossification has focused on the use of articular cartilage [24,25], a tissue that is known to be highly stable during adult life [26]. Conversely, when considering fracture repair it is likely that a source of cartilage which undergoes hypertrophy and ossification postnatally may offer significant advantages over articular cartilage [27–29]. Postnatally, costal cartilage represents a plentiful source of cartilage that undergoes these changes. Costal cartilage is a hyaline cartilage tissue associated with the ribs and contains a region of hypertrophic chondrocytes [30], thus replicating the developmental bone forming cartilage and the postnatal fracture callus. Interestingly, despite costal cartilage undergoing slow bone formation physiologically in the rib environment, if transplanted subcutaneously it undergoes rapid endochondral remodelling [31].

Herein, we hypothesise that an optimised decellularisation of costal cartilage will result in non-immunogenic scaffolds that retain the native structure and desirable biological components required to control endochondral ossification.

2. Materials and methods

2.1. Costal cartilage harvest

Fresh porcine costal cartilage was obtained from Large-White/Landrace crossbred pigs ranging from 40 to 70 Kgs (being terminated from unrelated studies at Northwick Park Institute for Medical Research; NPIMR, London, UK; approximately 8 ribs were harvested from each pig; n=5). Lateral thoracic incisions were made and the soft tissue excised and cleared to expose the costal regions of the rib cage. Costal cartilage directly adjacent to the bone tissue was isolated from the rib cage. Any remaining adherent soft tissue was

5

removed using a sterile scalpel and the harvested costal cartilage placed in sterile plastic bags and stored immediately at -20°C.

2.2. Development of decellularisation methodology

Frozen costal cartilage samples were defrosted at room temperature. The cartilage tissue was dissected into discs measuring 10 mm in diameter and 1 mm in height, with a volume of 78.5 mm^3. These discs were allotted into three groups each containing five discs. These groups were subjected to three independent decellularisation methodologies (detailed in Supplementary Table 1). All the methodologies were carried out under negative pressure at 2000 μmHg (267 Pa), using a negative pressure desiccator (Sigma-Aldrich, Dorset, UK). All decellularisation methods utilised 250 mL of solution per step. All methodologies also included a nuclease digestion step to eliminate nucleic acids. The DNAse/RNAse buffers contained 10 mM $CaCl_2$ and 60 mM $MgCl_2$, required for the activity of nucleases. This step was carried out at 37°C under agitation using an orbital shaker (ThermoFisher, Bedford, UK). All non-enzymatic steps were carried out at 4-8ºC.

Vac-OS methodology adapted from Greco and colleagues [32] utilised a freeze/thaw cycle to initiate cell disruption, followed by the use of hyper- and hypotonic steps in order to facilitate cell lysis. Washing with wash buffer containing Tween-20 (Sigma-Aldrich, Dorset, UK) was incorporated between each step to aid the removal fragmented cellular components.

Vac-STx methodology adapted from Lange and colleagues [33] utilised a freeze/thaw cycle to initiate cell disruption, followed by a combination of sodium deoxycholate (SDC) (Sigma-Aldrich, Dorset, UK) and Triton-X100 (Sigma-Aldrich, Dorset, UK) in order to facilitate cell lysis and the removal of cellular components, respectively.

Vac-SDS methodology utilised sodium dodecyl sulphate (SDS), a zwitterionic detergent that solubilises cell membranes and dissociates DNA from proteins along with hyper- and hypotonic solutions to further aid with cellular component fragmentation and removal.

6

All samples processed through each of the decellularisation methodologies were either preserved in PBS for DNA and GAG (n=3) analysis or fixed in 10% neutral buffered formalin-saline (NBF) for histological analysis (n=3).

2.3. Assessment of cellular content removal

2.3.1. Histological analysis

Histological examination was used to assess cellular clearance and gross tissue morphology. Briefly, samples from each of the methodologies, along with a control sample, were fixed in 10% NBF for 24 hours at room temperature. The samples were processed for paraffin wax embedding using routine histological techniques. Subsequently, 5 μM thickness paraffin sections were cut using a rotary microtome (ThermoFisher, Bedford, UK). The sections were mounted onto poly-lysine coated histology slides (ThermoFisher, Bedford, UK) and stained with haematoxylin and eosin according to routine procedures. Additional sections were stained with 4', 6-diamidino-2-fenylindool (DAPI) and visualised using inverted Axio fluorescence imager (Zeiss, UK). Nuclei were quantified using ImageJ (NIH). Based on histological examination the Vac-SDS was eliminated at this stage from further analysis.

2.3.2. DNA quantification.

To assess the quantity of DNA present, cartilage samples were cryomilled using a SPEXSamplePrep 6775 freezer mill (SPEX, London, UK) into a homogenous paste. 25 mg of the resultant paste was transferred to DNase/RNase free microcentrifuge tubes. The total DNA of the samples was isolated using the GenElute mammalian genomic DNA miniprep kit (Sigma-Aldrich, Dorset, UK) in accordance with the manufacturer's instructions and eluted in 50 μL nuclease-free water. The eluted DNA was quantified using the NanoDrop ND1000 spectrophotometer by absorbance (ThermoFisher, Bedford, UK) and normalised to the wet mass of each sample. Based on DNA and GAG quantification the Vac-STX condition was eliminated from further analysis and the Vac-OS methodology selected as the optimal methodology.

7

2.3.3. Protein extraction and Western blotting for alpha-Gal content.

Western blot analysis was utilised to determine the presence of the Alpha-Gal epitope. Briefly, Control cartilage, muscle and Vac-OS decellularised cartilage (dcECM) were cryomilled using a SPEXSamplePrep 6775 freezer mill (SPEX, London, UK) to form a paste. To further solubilise, 200 mg of the sample paste was combined with 1 mL of RIPA buffer (Sigma-Aldrich, Dorset, UK) and frozen at -80°C until analysed. The total protein content of the lysate was quantified using a BCA protein assay kit (ThermoFisher, Bedford, UK) in accordance with the manufacturer's instructions. 10 µg of the protein was combined with 2 x Laemmli sample buffer in a 1:1 ratio containing β-mercaptoethanol (Sigma-Aldrich, Dorset, UK) and size fractionated using SDS-PAGE, run on Mini-PROTEAN® TGX™ Precast Gels (Biorad, Herts, UK) followed by electrotransfer using the Trans-Blot® Turbo™ Mini PVDF Transfer Packs (Biorad, Herts, UK). The transferred proteins were stained using 1% Ponceau S (Sigma-Aldrich, Dorset, UK) for 1 hour. The blots were then blocked using 3% filtered bovine serum albumin (Sigma-Aldrich, Poole, UK), and incubated overnight at 4°C with an antibody against Alpha-Gal (EnzoLifeSciences, Exeter, UK) at 1:500 dilution. A secondary anti-mouse HRP conjugated antibody (VectorLabs, Cambs, UK) was then added to the blot at the concentration of 1:1000 and incubated for 1 hour at room temperature. Detected proteins were visualised using Clarity™ Western ECL Blotting Substrate (Biorad, Herts, UK) and images were obtained using ChemiDocXRS+ (Biorad, Herts, UK).

2.4. Analysis of matrix components

2.4.1. Sulphate glycosaminoglycan (sGAG) Quantification.

The sGAG content in both control cartilage samples and decellularised samples were measured using the Blyscan s-GAG assay kit (Biocolor, Ireland). Briefly, each sample was cryomilled using a SPEXSamplePrep 6775 freezer mill (SPEX, London, UK) and 50mg of the sample was placed in 1.0 mL papain digestion buffer containing 400 mg sodium acetate, 200 mg EDTA disodium salt, 40 mg cysteine HCL and 0.1mg papain for 12 hours at 65°C with occasional mixing. The digests were centrifuged at 13,000 rpm for 10 minutes. 50 µL of each digest supernatant was mixed with 1.0 mL Blyscan dye reagent. The samples were mixed for 30 minutes using an orbital shaker (IKA, Staufen, Germany), followed by

8

centrifugation at 13,000 rpm for 10 minutes to obtain a pellet containing insoluble sGAG-dye complex. 0.5 mL of dissociation reagent was added to each tube and centrifuged at 13,000 rpm for 5 minutes. A standard curve was generated with 50 µL serial dilutions ranging from 0.0-5.0µg/mL of chondroitin sulphate in distilled water. The standards and samples were mixed with 1.0 mL Blyscan dye reagent and 200 µL of each transferred into clear flat bottom 96-micro well plates in triplicate. The absorbance was measured using a Tecan Infinite M200pro microtiter plate reader (Tecan, Männedorf, Switzerland) at 656 nm. Absolute sGAG content in µg/mL was determined and samples normalised to the wet mass of each sample.

2.4.2. Differential scanning calorimetry (DSC).

DSC was used to measure collagen denaturation temperatures as an indicator of the structural integrity of the matrix. Control native cartilage samples were compared to dcECM samples. Briefly, 10 mg of each sample was placed into 40 µL aluminium crucibles. The calorimetric experiments were performed using Mettler Toledo DSC-1 calorimeter (Mettler Toledo, Greenfield, UK). All experiments were performed between 25°C and 95°C at a heating rate of 3°C/min. The readings were normalised to an empty reference crucible.

2.4.3. Multiphoton imaging

Second harmonic generation and fluorescence-lifetime imaging microscopy (FLIM) were used to measure changes in the collagen biochemical environment as a measure of matrix integrity. Native costal cartilage and dcECM were placed in PBS in preparation for imaging. Laser scanning microscopy with multiphoton excitation was carried out using a Zeiss LSM 510 microscope (Zeiss, Oberkochen, Germany) with a 10x 0.3 N.A water-dipping objective and the 80 MHz pulsed output of a Chameleon (Coherent, Santa Clara, USA) Ti:sapphire laser. Second harmonic generation and autofluorescence were observed using 920 nm and 720 nm illumination wavelengths respectively. In both imaging modalities, a 650 nm dichroic filter separated the two-photon excitation from the shorter wavelength emission, collected with a 460(±25) nm band-pass filter before detection by a high-speed hybrid detector (HPM-100), (Becker & Hickl, Berlin, Germany). Single photon emission events

were recorded by a commercial time-correlated single photon counting SPC-830 electronics module (Becker & Hickl, Berlin, Germany) in a desktop computer. Fluorescence lifetimes were extracted from the measured time-resolved emission data by least-squares fitting of a monoexponential decay in SPCImage (Becker & Hickl, Berlin, Germany).

2.5. *In vitro* biocompatibility of dcECM

2.5.1 Human articular chondrocyte isolation.

Human cartilage was harvested from the articular surfaces of the knee and hip from patients undergoing joint replacement surgeries. Articular chondrocytes were extracted from cartilage using a methodology that was adapted from previous studies [34–37]. Briefly, two grams of cartilage were finely minced and placed into a collagenase type IV (consisting of 4400 enzyme activity units) digestion buffer containing growth medium (GM) consisting of high-glucose Dulbecco's Modified medium supplemented with 10% foetal bovine serum (FBS) (Invitrogen, Paisley, UK), 1 mM sodium pyruvate (Invitrogen, Paisley, UK) and antibiotic-antimycotic solution (100 units/mL penicillin, 100 µg/mL streptomycin and 0.25 µg/mL amphotericin B; Invitrogen, Paisley, UK) for 16 hours. The digest was passed through a 70µM cell strainer and centrifuged at 1300 rpm for 10 minutes. The resultant chondrocyte pellet was resuspended in growth medium and expanded in monolayer until passage 2 and cryopreserved. Informed consent was obtained preoperatively from each patient in accordance with the approval from the Ethical Committee of the Royal National Orthopaedic Hospital in compliance with the United Kingdom Human Tissues Act 2004.

2.5.2. Chondrocyte seeding and micromass culture.

Human primary articular chondrocytes were thawed, sub-cultured and upon confluence at passage 3, were seeded in micromass cultures directly onto the plastic surface or onto dcECM at a density of $5x10^5$ per 100 µL of growth media into the centre of a well. Micromass culture is extensively used in chondrogenic differentiation protocols as it effectively mimics cell aggregation and allows an intra-aggregate environment to be acquired that is permissive for differentiation[38]. These events mimic those that occur *in vivo* during limb development. Briefly, dcECM was cut into 6 mm diameter and 1 mm thick

10

sections using a biopsy punch (ThermoFisher, Bedford, UK). 5×10^5 chondrocytes in 10 µL of growth media were seeded onto the surface of the dcECM, whereby the low seeding volume aided localisation of the cells on the surface of the dcECM until attachment. Cells were seeded in micromasses and onto the dcECM surface at the same density. The cells were left for 3 hours to attach, following which 2 mL of growth media supplemented with 5% FBS was added, micromasses were cultured in these conditions for a period of 7 days (n=3 per group). The media in each well was replaced daily with fresh growth media.

2.5.3. Human periosteal stem cells (hPDSCs).

hPDSCs were isolated as previously described [37] (obtained from Prof Frank Luyten, KU Leuven, Belgium). Subsequently, hPDSCs from a pool of six different donors were expanded to passage 5. All experiments described herein were performed in pooled hPDSCs at passage 6.

2.5.4. hPDSC seeding and micromass culture.

Micromass cultures (MM) were seeded as previously described. Briefly, hPDSCs (passage 6) were seeded at a cell density of 1×10^6 per 100 µL of growth media into 96-well plates. Cells were seeded at this density onto the dcECM as previously described and allowed to attach for 3 hours before being treated with various chondrogenic media. The cells seeded in micromasses and on the dcECM were segregated into 3 media condition groups (n=3 per group). The control group was treated with low glucose DMEM (Invitrogen, Paisley, UK) supplemented with 2% FBS, (Invitrogen, Paisley, UK) and antibiotic-antimycotic solution (100 units/mL penicillin, 100 µg/mL streptomycin and 0.25 µg/mL amphotericin B; Invitrogen, Paisley, UK). The second group consisted of basal chondrogenic group or C(-) group consisting of low-glucose DMEM (Gibco, UK) supplemented with 100µM ascorbate-2-phosphate (Sigma-Aldrich, Dorset, UK), 100nM dexamethasone (Sigma-Aldrich, Dorset, UK), 40 mg/mL proline (Sigma-Aldrich, Dorset, UK), and ITS+premix universal culture supplement (BD Biosciences, Bedford, MA) and 10 µM of Y27632 (Axon Medchem, Groningen, Netherlands). The final group consisted of chondrogenic or C(+) group containing basal chondrogenic media supplemented with 10 ng/mL of TGF-β.

11

2.5.5. Total RNA extraction and quantitative reverse transcription–Polymerase Chain Reaction (qRT-PCR) analysis.

Total RNA was extracted using the Trizol method. Briefly, seeded dcECM constructs were washed with PBS, placed in 350 µL of Trizol (Invitrogen, Paisley, UK) and homogenised. Total RNA was isolated from each of the micromasses and dcECM using the Direct-zol RNA MiniPrep (Cambridge Biosciences, Cambs, UK) according to the manufacturers' instructions. Total RNA isolated was quantified using the Nanodrop 1000 spectrophotometer (ThermoFisher, Bedford, UK). Complementary DNA (cDNA) was synthesised by reverse transcription of 200ng of total RNA using the high capacity cDNA reverse transcription kit (Applied Biosciences, ThermoFisher, Bedford, UK). To detect messenger RNA (mRNA) transcripts, primers (exon spanning, designed using Primer3 Plus, NCBI) were premixed with iTaq universal SYBR green supermix (Biorad, Herts, UK) and 10 µL aliquots were applied to Hard-Shell® 96-Well PCR Plates (Biorad, Herts, UK). Thermal cycling conditions were as follows: 10 min at 95°C, with 40 cycles of 15 seconds at 95°C, 30 s at 60°C, and 20s at 72°C, on a Bio-Rad CFX1000 Real-Time System (Biorad, Herts, UK). Target gene quantification was achieved using the $2^{-\Delta\Delta CT}$ method described by Livak *et al* [39] relative to *hPRT1* as the housekeeper gene. Primer sequences are listed in Supplementary Table 2.

2.6. *In vivo* biocompatibility

6-week old BALB/C mice were purchased from Charles River, UK and were housed in polypropylene cages at 21°C (±2°C), subjected to 12-hour light and dark cycles, and were acclimatised for one week prior to use. Mice were fed a standard RM1 maintenance diet *ad libitum* (Rat and Mouse No.1; Special Diet Services). All procedures were conducted in accordance with the United Kingdom Animal Scientific Procedures Act, 1986 and were approved by the Ethics and Welfare Committee of the Comparative Biology Unit, Royal Free and University College London Medical School, London.

Mice were anesthetised (3–5% isoflurane, O₂ flow rate of 1.0 mL/min) and two 8 mm dorsal incisions created per mouse. The subcutaneous pockets on each mouse were filled with either two dcECM constructs or two native cartilage constructs (6mm in diameter and

12

1mm thick). The incisions were then sutured with Vicryl Rapide sutures (Ethicon, UK). After 2 and 8 weeks of implantation, mice were sacrificed by CO_2 inhalation. The dorsal skin was carefully resected and implants retrieved. The dcECM and native cartilage tissue were fixed in 10% neutral buffered formalin (pH 7.4) (VWR, UK) for 24 hours at room temperature.

The 10% NBF fixed tissues ((n=4) dcECM; (n=4) native costal cartilage), 2 and 8 weeks respectively) were dehydrated in graded alcohol, embedded in paraffin, and sectioned at 5 μm. Immunohistochemical analysis of CD68 (Pan-macrophage marker; Abcam, Cambridge, UK), CD86 (M1 macrophage marker; Abcam, Cambridge, UK), and CD163 (M2 macrophage marker; Abcam, Cambridge, UK) was performed following deparaffinization and rehydration of the tissue sections. All sections were blocked in 2.5% horse serum (VectorLabs, Cambs, UK) and 3% H_2O_2 (Sigma-Aldrich, Dorset, UK). For CD68 and CD163 detection, antigen retrieval was performed by incubation with Tris-EDTA buffer (10 mM Tris base, 1 mM EDTA solution, 0.05% Tween 20, pH 9.0) at 60°C overnight. Antigen retrieval for CD86 was performed by incubation with proteinase K (Proteinase K ready to use solution (Dako, UK)) for 2 minutes at room temperature. Sections were then incubated with primary anti-CD68 (1:500 rabbit polyclonal anti-mouse; VectorLabs, Cambs, UK), anti-CD86 (1:500 mouse monoclonal anti-mouse; VectorLabs, Cambs, UK) and anti-CD163 (1:500 rabbit polyclonal anti-mouse; VectorLabs, Cambs, UK) at 4°C overnight. Subsequently, CD86 and CD163 sections were incubated with HRP-conjugated anti-rabbit secondary antibody solution (VectorLabs, Cambs, UK), CD86 sections were incubated with HRP-conjugated anti-mouse secondary antibody solution (VectorLabs, Cambs, UK) for 1 hour at room temperature. All targets were visualised by incubation with the substrate 3,3'-diaminobenzidine (VectorLabs, Cambs, UK) for 1 minute. Tissue sections were counterstained with Haematoxylin solution (Sigma-Aldrich, Dorset, UK) and visualised using the Zeiss Apotome.2 microscope under bright field settings (Zeiss, UK).

2.7. Statistical analysis

Data are expressed as the mean ± standard deviation (SD). Statistical significance was determined using one-way analysis of variance (ANOVA) with Bonferroni's posthoc

13

corrections applied and Student's t-test with Welch's posthoc corrections applied to compare between independent groups. Statistical significance is indicated on all graphs as follows: *p<0.05, **p<0.01, ***p<0.001 (n=3). All statistical analysis was performed using GraphPad Prism version 6.0f for windows (GraphPad Prism Software, La Jolla California USA, www.graphpad.com).

3. Results

3.1. An optimised Vac-OS decellularised methodology results in the effective removal of cellular components.

Light microscopy of H&E stained sections revealed that all methodologies resulted in some level of cellular clearance, with the Vac-OS and Vac-STx methodologies resulting in the greatest clearance (Fig 1A). This was further validated through nuclear staining with DAPI and subsequent quantification (Fig 1B). The Vac-SDS based methodology resulted in an 89.5% (p<0.001) reduction in DAPI positive nuclei. The Vac-STx and Vac-OS methodologies were the most effective at clearing cellular and nuclear content from the cartilage samples as evidenced by a 100% (p<0.001) reduction in visible DAPI positive nuclei. These two methodologies were therefore chosen for further characterisation and assessment.

3.2. Vac-OS decellularisation results in superior sGAG retention and the efficient removal of the Alpha-Gal epitope.

To validate the effective removal of cellular and nuclear content from the decellularised cartilage samples the DNA content of the tissue was analysed. Total DNA content in Vac-OS and Vac-STx decellularised samples were quantified in 78.5 mm^3 (small) and 785 mm^3 (large) sized cartilage pieces, normalised to tissue wet weight and compared to the control native costal cartilage samples. There was no significant difference in DNA content between the small and large samples with either of the methodologies employed. Furthermore, DNA content in both Vac-OS and Vac-STx decellularisation methodologies (Fig 2; A&B) resulted in values falling below the clinically acceptable level of 50 ng/mg (p<0.0001) threshold [22] for both tissue sizes.

14

Despite the similarity in DNA content, distinct differences in sGAG retention (Fig 2; C&D) between the two methodologies and tissue volumes were observed. Tissue subjected to the Vac-OS methodology retained 85.79% (p<0.05) and 28.2% (p<0.001) sGAG for the large and small volumes, respectively; when compared to control cartilage tissue. Tissue subjected to the Vac-STx methodology, however, retained 57.64% (p<0.001) and 16.64% (p<0.001) for the large and small volumes, respectively. The results indicated that the Vac-OS decellularisation methodology resulted in 28.15% (p<0.001) greater sGAG content retention compared to the Vac-STx methodology, when considering the larger volumes. This difference in sGAG retention was not observed between the two methodologies in the smaller tissue volume. The Vac-OS decellularisation with larger tissue volumes was thus selected as the optimal methodology for costal cartilage and subjected to further analysis.

The presence of alpha-Gal epitope, which is an abundant immunogenic component found on the cell surface of all non-primate species, was investigated [40]. Immunoblotting revealed a 56 kDa band, indicating alpha-Gal was present (Fig 2F; protein loading is shown in Fig 2E) in control muscle (lanes 1&2) and cartilage tissues (lanes 3&4), but was absent in the Vac-OS decellularised sample groups (lanes 5, 6, & 7).

3.3. Matrix analysis indicates minimal disruption to the Vac-OS decellularised matrix.

The matrix integrity of the Vac-OS decellularised samples was further assessed using thermal analysis to determine collagen denaturation temperatures, thus indicating collagen structural integrity. These analyses were compared to the collagen denaturation temperatures obtained from native costal cartilage. This analysis indicated that there were no significant changes in the denaturation temperatures between the dcECM compared to native costal cartilage (Fig 3; A&B). This was further reflected in the matrix analysis carried out using multiphoton imaging techniques (Fig 3C-F). The highly noncentrosymmetric structure of fibrillar collagen gives rise to intense second harmonic generation when exposed to a high-intensity coherent light source [41]. This allows collagen structures to be imaged using laser scanning microscopy by observing light emitted from a sample at half the wavelength of the incident illumination. Collagen also possesses intrinsic fluorescence properties due to the presence of a range of spectrally-overlapping endogenous

15

fluorophores [42]. Changes in the nanoscale local environment of these fluorophores are reflected by alterations in their fluorescence lifetime[43], the average time taken for emission to occur following excitation. Combining second harmonic and fluorescence lifetime imaging would allow the assessment of morphological changes within the extracellular matrix. Remarkably, there was no significant difference between control and dcECM fluorescence lifetimes, suggesting minimal changes in the biochemical environment of the extracellular matrix following the Vac-OS decellularisation process compared to native cartilage (Fig 3F). In contrast, dcECM treated with collagenase demonstrated both reduced collagen denaturation temperatures and altered fluorescence lifetimes (Supplementary Fig 1).

3.4. dcECM promotes chondrogenic differentiation of skeletal cells.

To assess the capacity for cell attachment and promotion of a chondrogenic phenotype, de-differentiated human chondrocytes were seeded onto the dcECM (Fig 4). Cell attachment onto the dcECM was illustrated by nuclear and cytoskeletal staining (Fig 4A), revealing that the attached cells migrated into the vacant chondrocyte lacunae. Furthermore, the establishment of a chondrogenic phenotype of seeded cells was confirmed by a significant 4-fold (p<0.01) increase in *COL2A1* mRNA expression associated with cartilage matrix maintenance (Fig 4B). There was no significant difference in chondrogenic commitment marker *SOX9* mRNA expression. To further examine the chondrogenic potential of the scaffolds, hPDSCs were seeded onto the dcECM and in micromasses, and examined for cell attachment (Fig 4C). Cells within micromasses under control conditions appeared more elongated with fibroblast-like morphology, whilst those under C(+) conditions (containing TGF-β) displayed a more distinct rounded morphology indicative of chondrocytic phenotype after 7 days (Fig 4C). To understand these observations and assess the interaction of the cells with the dcECM, hPDSCs seeded onto the dcECM and in micromasses were either stimulated with C(+) or cultured under control conditions. Chondrogenic gene marker expression after 7 days was assessed (Fig 4D). There was no significant change in any of the markers between cells seeded onto the dcECM and micromasses under control conditions. In contrast, under chondrogenic (C+) conditions there was a significant upregulation of the *SOX*-trimer; *SOX9*; *SOX5* and *SOX6*

16

with a 3-, 5- and 3.6-fold (p<0.001, p<0.05, p<0.01), respectively compared to micromasses. Furthermore, under chondrogenic C(+) conditions an 8- and 4-fold (p<0.01, p<0.01) upregulation in cartilage matrix specific markers *ACAN* and *COL2A1* were observed. This was also accompanied by the potent upregulation of markers associated with chondrocyte hypertrophy with a 2- and 2.9 fold (p<0.05, p<0.05) increase in *RUNX2* and *COL10A1* expression. The importance of the TGF-β1 driven C(+) condition for enhanced chondrogenesis and hypertrophy was demonstrated through the comparison of the seeded dcECM in C(+) to the seeded dcECM in control conditions. These data demonstrated a potent 3.4-, 3.6-, 18- and 2896-fold (p<0.01, p<0.01, p<0.01, p<0.001) upregulation in *SOX9*, *SOX6*, *ACAN* and *COL2A1*, respectively. Enhanced hypertrophy was confirmed by a 24-fold (p<0.001) upregulation in *COL10A1* mRNA expression. There was no significant change in any of the markers investigated in hPDSCs subjected to the C(-) culture conditions (that contained no TGF-β1), in both micromass and dcECM cultures (Data not shown).

3.5. Subcutaneously implanted dcECM elicits a predominantly M2 macrophage-mediated anti-inflammatory regenerative response.

The dcECM was subcutaneously implanted into mice to assess the *in vivo* immune response in comparison to native costal cartilage tissue. Explanted samples were subjected to immunohistochemical (IHC) analysis for CD68 (Pan-macrophage marker), CD86 (M1-macrophage marker) and CD163 (M2-macrophage marker) (Fig 5). Qualitative analysis of the stained sections revealed a similar CD68 positive immune cell presence within the fibrous tissue (FT) that bordered the implant, between both the native costal cartilage and the dcECM at 2 and 8 weeks. After a period of 8 weeks, however, there was an observed decrease in CD86 staining with the dcECM compared to the 2-week samples and native samples at this time point. Another distinct observation was the presence of CD163 positive cells in the FT surrounding the dcECM both at the 2 and 8-week time points, compared to the native cartilage samples. This indicates a predominantly M2 macrophage-mediated immune response towards the dcECM.

17

4. Discussion

There is currently an unmet clinical need for treatment approaches aimed at enhancing the fracture repair process for the treatment of fracture non-union. Herein, we describe the production of innovative hyaline cartilage scaffolds that retain the native ECM architecture and biological cues required to enhance skeletal cell differentiation.

Effective decellularisation is reliant on the efficient elimination of immunogenic cellular components without interfering with the intended biological function of the resultant ECM scaffold. This is particularly challenging with dense avascular tissues such as cartilage [44,45]. Recent studies applying vacuum-assisted decellularisation demonstrate increased decellularisation efficiency, especially with respect to complex organs that include dense tissues i.e. trachea and larynx [33,46]. The enhanced cellular clearance reduces the need for harsh physical or enzymatic treatments that may contribute to the loss of bioactive molecules from the ECM [33,46]. Similarly, osmotic shock has also been applied towards the efficient decellularisation of dense tissues with minimal ECM disruption[32,47] and was therefore combined with vacuum assistance to formulate the optimised Vac-OS methodology (Supplementary Table 1) used in this study. This methodology (Vac-OS) was also compared to previously used vacuum-assisted decellularisation (Vac-STx) that incorporated the detergents triton-x and sodium deoxycholate (SDC) [33]. Interestingly, despite the Vac-OS methodology lacking any ionic surfactants, the resultant scaffolds (dcECM) exhibited DNA content falling below levels that are known to be immunogenic *in vivo* [22]. In addition, enhanced sGAG retention was also observed with the Vac-OS methodology compared to both the Vac-STx and other published methodologies aimed at decellularising cartilaginous tissues [25,48].

sGAGs are present in various tissue types but are especially abundant in cartilaginous ECM, serving as both structural and functional components [26,49]. Besides their role in ECM homoeostasis [50], sGAGs have also been associated with their ability to drive chondrogenesis [51–53] and in the regulation of endochondral ossification [54]. Therefore, the maintenance of sGAG content is essential when developing a scaffold with a capacity for endochondral ossification from cartilage tissue. Indeed, the Vac-OS methodology

18

allowed for the retention of up to 85% of the native sGAG content, which was observed specifically when tissue volume was upscaled by a factor of ten. The synergy between osmotic shock and vacuum assisted decellularisation was further highlighted by the enhanced retention of GAGs compared to the Vac-STx methodology. These findings suggest that the disruptive and proteolytic nature of ionic surfactants such as SDC[55] may be key facilitators of sGAG loss. Indeed, several other studies that employ the use of ionic surfactants and enzymes report similar findings [25,56,57].

A key promoter of xenogeneic transplant rejection is the alpha-gal epitope, which is a cellular component found on all non-primate species and is known to elicit an acute inflammatory response in humans. [40]. Therefore, the reduction or elimination of this key antigen is essential for clinical translation [58–60]. Moreover, the presence of residual alpha-gal in commercially available xenografts has been shown to have negative clinical outcomes[61–63]. Encouragingly, the high level of alpha-gal present within native costal cartilage tissue was successfully reduced below detectable levels by the Vac-OS methodology.

The ECM structure and 3D spatial arrangement of macromolecules both play a vital role in cellular adhesion, stem cell fate determination and *in vivo* tissue remodelling [64–66]. Maintenance of ECM structure should, therefore, be thoroughly considered during the development decellularisation methodologies. Most studies utilise standard histological techniques for the assessment of decellularised cartilaginous matrices, which only allow for the gross examination of matrix architecture [67,68]. Therefore, DSC was used to gain an enhanced understanding of the dcECM collagen integrity. Interestingly, it has previously been reported that alterations in articular cartilage matrix integrity between healthy and osteoarthritic cartilage are reflected by variations in the collagen denaturation temperatures [69]. Therefore, the unaffected collagen denaturation temperatures between the native costal cartilage and the dcECM are reflective of the preservation of collagen ultrastructure post Vac-OS. Unfortunately, DSC is destructive and only provides a global view of matrix integrity, hence, FLIM was utilised as an alternative approach to monitor subtle changes in the ECM. It is widely accepted that site-specific changes in collagen cross-linking can be identified through imaging techniques that quantify the

19

lifetimes of collagen auto-fluorescence [70]. In agreement with the DSC data, the FLIM analysis did not uncover any significant changes in collagen fluorescence lifetimes between the dcECM scaffolds and native costal cartilage. To our knowledge, this is the first report of FLIM being used to assess matrix integrity of decellularised ECM that could be widely applied in the nondestructive monitoring of tissue during the optimisation of decellularisation approaches.

The successful clinical application of a tissue-engineered implant depends on its ability to attract and direct tissue-specific remodelling via its interaction with surrounding stem cell populations. Chondrocytes are a cell type native to hyaline cartilage and are involved in cartilage homoeostasis [71], however, they are known to rapidly lose their chondrocytic phenotype following culture in monolayer[72,73]. Interestingly, dcECM promoted the re-establishment of a chondrogenic phenotype from culture expanded (dedifferentiated) chondrocytes, indicated by a significant upregulation of *COL2A1*expression. This is potentially the result of the retention of sufficient sGAG content [49,74,75], an undisrupted ECM ultrastructure [76] and, although not investigated in this study, the presence of remnant growth factors such as TGF-β [77], BMP2 [78], FGF-2 and FGF-18 [79]. To further elucidate the chondrogenic capacity of dcECM, human periosteal stem cells (hPDSCs), which are essential for fracture repair [80–83], were investigated. When combined with the dcECM, hPDSCs significantly upregulated expression of the chondrocyte genes *SOX9*, *SOX5*, *SOX6*, *COL2A1* and *ACAN*. Interestingly, there was also a upregulation of *COL10A1*, *RUNX2 and VEGFA,* which are representative of chondrocyte hypertrophy [10,84,85]. Moreover, these events were detected following a period of just 7 days. Interestingly, the upregulation of chondrogenic and hypertrophic markers were only observed in seeded dcECM constructs, cultured in conditions containing TGF-β. This may be due to the ability of the retained GAGs to sequester exogenously added TGF-β, thus enhancing its chondrogenic potential [49,74,75].

For the successful translation of tissue engineered constructs, they must elicit a favourable immune response upon implantation, whilst avoiding a pro-inflammatory response that could hinder the natural tissue repair cascade and/or result in tissue rejection. The immunogenicity of the dcECM was therefore assessed *in vivo* through subcutaneous

20

implantation into immunocompetent mice. The dcECM demonstrated a predominantly M2 biased response at 2 and 8 weeks, which is indicative of favourable long-term outcomes and tissue-specific remodelling [86]. This was in contrast to the native costal cartilage comparator that demonstrated a predominantly M1 mediated response, which is linked to the initiation of inflammation. This further supports the *in vitro* analysis that demonstrates the effective removal of immunogenic factors.

The validity of using decellularised cartilage tissue as an endochondral substrate has been previously demonstrated by Gawlitta and colleagues [25] and Cunniffe and colleagues [27]. The choice of articular cartilage-derived scaffolds used in the study by Gawlitta is, however, questionable as articular cartilage is highly stable during adult life, except in disease conditions [87]. Indeed, factors such as chondromodulin 1 (ChM-I) have been implicated in the stability of articular cartilage by inhibiting angiogenesis [88], a process essential for endochondral fracture healing [2]. Furthermore, Cunniffe and colleagues demonstrated that only scaffolds derived from *in vitro* hypertrophic chondrocyte ECM promoted vascularisation, induced mineralization and promoted bone formation[27]. Their use of cell-derived cartilage scaffolds, however, will pose major challenges when considering the fabrication of constructs of a clinically viable size [27,89,90]. Work carried out by Scotti and colleagues attempted to overcome this limitation by upscaling the size of previously developed cell constructs [89] through the addition of a collagen type I scaffold [91]. Although the approach yielded constructs capable of undergoing endochondral ossification, the efficacy of the process still remains highly reliant on an abundant stem cell population and extended culture periods.

5. Conclusion

To our knowledge, this is the first study that details the applicability of decellularised xenogeneic costal cartilage for the fabrication of fracture callus mimetic scaffolds. Herein, a vacuum-assisted decellularisation methodology that allows for the rapid fabrication of non-immunogenic costal cartilage-derived scaffolds capable of directing cell fate is described. The presented data indicate that the dcECM is capable of enhancing chondrogenic differentiation of skeletal cells and elicits a regenerative response upon

21

implantation in an immunocompetent host. The aforementioned characteristics demonstrate that the produced constructs may act as biomimetic implants that replicate several features of the fracture callus. It is hypothesised that these constructs could enhance bone repair in cases of atrophic nonunion fracture, where the failure of callus formation is a defining event.

Acknowledgements

22

References

[1]   L.C. Gerstenfeld, D.M. Cullinane, G.L. Barnes, D.T. Graves, T. a. Einhorn, Fracture healing as a post-natal developmental process: Molecular, spatial, and temporal aspects of its regulation, J. Cell. Biochem. 88 (2003) 873–884. doi:10.1002/jcb.10435.

[2]   T. a Einhorn, The science of fracture healing., J. Orthop. Trauma. 19 (2005) S4–S6. doi:10.1097/00005131-200511101-00002.

[3]   R. Marsell, T. a. Einhorn, The biology of fracture healing, Injury. 42 (2011) 551–555. doi:10.1016/j.injury.2011.03.031.

[4]   A. Biasibetti, D. Aloj, G. Di Gregorio, A. Masse, C. Salomone, Mechanical and biological treatment of long bone non-unions, Injury. 36 Suppl 4 (2005) S45-50. doi:10.1016/j.injury.2005.10.013.

[5]   E. Gómez-Barrena, P. Rosset, D. Lozano, J. Stanovici, C. Ermthaller, F. Gerbhard, Bone fracture healing: Cell therapy in delayed unions and nonunions, Bone. 70 (2015) 93–101. doi:10.1016/j.bone.2014.07.033.

[6]   M.K. Sen, T. Miclau, Autologous iliac crest bone graft: Should it still be the gold standard for treating nonunions?, Injury. 38 (2007) 2–7. doi:10.1016/j.injury.2007.02.012.

[7]   R.C. Kinney, B.H. Ziran, K. Hirshorn, D. Schlatterer, T. Ganey, Demineralized bone matrix for fracture healing: fact or fiction?, J. Orthop. Trauma. 24 Suppl 1 (2010) S52-5. doi:10.1097/BOT.0b013e3181d07ffa.

[8]   E. Gruskin, B.A. Doll, F.W. Futrell, J.P. Schmitz, J.O. Hollinger, Demineralized bone matrix in bone repair: history and use., Adv. Drug Deliv. Rev. 64 (2012) 1063–77. doi:10.1016/j.addr.2012.06.008.

[9]   E.M. Thompson, A. Matsiko, E. Farrell, D.J. Kelly, F.J. O'Brien, Recapitulating endochondral ossification: A promising route to in vivo bone regeneration, J. Tissue Eng. Regen. Med. 9 (2015) 889–902. doi:10.1002/term.1918.

[10]   J. Dai, A.B.M. Rabie, VEGF: an essential mediator of both angiogenesis and endochondral ossification., J. Dent. Res. 86 (2007) 937–50. doi:10.1177/154405910708601006.

[11]   E. Farrell, O.P. van der Jagt, W. Koevoet, N. Kops, C.J. van Manen, C. a Hellingman, H. Jahr, F.J. O'Brien, J. a N. Verhaar, H. Weinans, G.J.V.M. van Osch, Chondrogenic priming of human bone marrow stromal cells: a better route to bone repair?, Tissue Eng. Part C. Methods. 15 (2009) 285–295. doi:10.1089/ten.tec.2008.0297.

[12]   E.J. Mackie, Y.A. Ahmed, L. Tatarczuch, K.-S. Chen, M. Mirams, Endochondral ossification: How cartilage is converted into bone in the developing skeleton, Int. J. Biochem. Cell Biol. 40 (2008) 46–62. doi:10.1016/j.biocel.2007.06.009.

[13]   D. Gawlitta, E. Farrell, J. Malda, L.B. Creemers, J. Alblas, W.J.A. Dhert, Modulating endochondral ossification of multipotent stromal cells for bone regeneration., Tissue Eng. Part B. Rev. 16 (2010) 385–95. doi:10.1089/ten.TEB.2009.0712.

[14]   C.S. Bahney, D.P. Hu, A.J. Taylor, F. Ferro, H.M. Britz, B. Hallgrimsson, B. Johnstone, T. Miclau, R.S. Marcucio, Stem cell-derived endochondral cartilage stimulates bone healing by tissue transformation., J. Bone Miner. Res. 29 (2014) 1269–82. doi:10.1002/jbmr.2148.

[15]   N. Harada, Y. Watanabe, K. Sato, S. Abe, K. Yamanaka, Y. Sakai, T. Kaneko, T. Matsushita, Bone regeneration in a massive rat femur defect through endochondral ossification achieved with chondrogenically differentiated MSCs in a degradable scaffold., Biomaterials. 35 (2014) 7800–10. doi:10.1016/j.biomaterials.2014.05.052.

[16]   A. Muraglia, A. Corsi, M. Riminucci, M. Mastrogiacomo, R. Cancedda, P. Bianco, R. Quarto, Formation of a chondro-osseous rudiment in micromass cultures of human bone-marrow stromal cells., J. Cell Sci. 116 (2003) 2949–55. doi:10.1242/jcs.00527.

[17]   M.P. Lutolf, J. a Hubbell, Synthetic biomaterials as instructive extracellular microenvironments for morphogenesis in tissue engineering., Nat. Biotechnol. 23 (2005) 47–55. doi:10.1038/nbt1055.

24

[18]   S.F. Badylak, The extracellular matrix as a biologic scaffold material., Biomaterials. 28 (2007) 3587–93. doi:10.1016/j.biomaterials.2007.04.043.

[19]   K.E.M. Benders, P.R. van Weeren, S.F. Badylak, D.B.F. Saris, W.J.A. Dhert, J. Malda, Extracellular matrix scaffolds for cartilage and bone regeneration, Trends Biotechnol. 31 (2013) 169–176. doi:10.1016/j.tibtech.2012.12.004.

[20]   C.W. Cheng, L.D. Solorio, E. Alsberg, Decellularized tissue and cell-derived extracellular matrices as scaffolds for orthopaedic tissue engineering, Biotechnol. Adv. 32 (2014) 462–484. doi:10.1016/j.biotechadv.2013.12.012.

[21]   W.J. Vas, M. Shah, R. Al Hosni, H.C. Owen, S.J. Roberts, Biomimetic strategies for fracture repair: Engineering the cell microenvironment for directed tissue formation, J. Tissue Eng. 8 (2017) 204173141770479. doi:10.1177/2041731417704791.

[22]   P.M. Crapo, T.W. Gilbert, S.F. Badylak, An overview of tissue and whole organ decellularization processes, Biomaterials. 32 (2011) 3233–3243. doi:10.1016/j.biomaterials.2011.01.057.

[23]   A. Gonfiotti, M.O. Jaus, D. Barale, S. Baiguera, C. Comin, F. Lavorini, G. Fontana, O. Sibila, G. Rombolà, P. Jungebluth, P. Macchiarini, The first tissue-engineered airway transplantation: 5-year follow-up results., Lancet (London, England). 383 (2014) 238–44. doi:10.1016/S0140-6736(13)62033-4.

[24]   J. Visser, D. Gawlitta, K.E.M. Benders, S.M.H. Toma, B. Pouran, P.R. van Weeren, W.J. a Dhert, J. Malda, Endochondral bone formation in gelatin methacrylamide hydrogel with embedded cartilage-derived matrix particles., Biomaterials. 37C (2014) 174–182. doi:10.1016/j.biomaterials.2014.10.020.

[25]   D. Gawlitta, K.E.M. Benders, J. Visser, A.S. van der Sar, D.H.R. Kempen, L.F.H. Theyse, J. Malda, W.J.A. Dhert, Decellularized Cartilage-Derived Matrix as Substrate for Endochondral Bone Regeneration, Tissue Eng. Part A. 21 (2015) 694–703. doi:10.1089/ten.tea.2014.0117.

25

[26] A.J. Sophia Fox, A. Bedi, S.A. Rodeo, The basic science of articular cartilage: structure, composition, and function., Sports Health. 1 (2009) 461–8. doi:10.1177/1941738109350438.

[27] G.M. Cunniffe, T. Vinardell, J.M. Murphy, E.M. Thompson, A. Matsiko, F.J. O'Brien, D.J. Kelly, Porous decellularized tissue engineered hypertrophic cartilage as a scaffold for large bone defect healing, Acta Biomater. 23 (2015) 82–90. doi:10.1016/j.actbio.2015.05.031.

[28] P.E. Bourgine, C. Scotti, S. Pigeot, L.A. Tchang, A. Todorov, I. Martin, Osteoinductivity of engineered cartilaginous templates devitalized by inducible apoptosis., Proc. Natl. Acad. Sci. U. S. A. 111 (2014) 17426–31. doi:10.1073/pnas.1411975111.

[29] K. Bardsley, A. Kwarciak, C. Freeman, I. Brook, P. Hatton, A. Crawford, Repair of bone defects in vivo using tissue engineered hypertrophic cartilage grafts produced from nasal chondrocytes., Biomaterials. 112 (2017) 313–323. doi:10.1016/j.biomaterials.2016.10.014.

[30] S. Bahrami, U. Plate, R. Dreier, A. DuChesne, G.H. Willital, P. Bruckner, Endochondral ossification of costal cartilage is arrested after chondrocytes have reached hypertrophic stage of late differentiation, Matrix Biol. 19 (2001) 707–715. doi:10.1016/S0945-053X(00)00125-6.

[31] H. Okihana, Y. Shimomura, Osteogenic activity of growth cartilage examined by implanting decalcified or devitalized ribs and costal cartilage zone, and living growth cartilage cells, Bone. 13 (1992) 387–393. doi:10.1016/8756-3282(92)90455-6.

[32] K. V Greco, L. Francis, M. Somasundaram, G. Greco, N.R. English, J.A. Roether, A.R. Boccaccini, P. Sibbons, T. Ansari, Characterisation of porcine dermis scaffolds decellularised using a novel non-enzymatic method for biomedical applications., J. Biomater. Appl. 30 (2015) 239–53. doi:10.1177/0885328215578638.

[33] P. Lange, K. Greco, L. Partington, C. Carvalho, S. Oliani, M.A. Birchall, P.D. Sibbons, M.W. Lowdell, T. Ansari, Pilot study of a novel vacuum-assisted method for

26

decellularization of tracheae for clinical tissue engineering applications., J. Tissue Eng. Regen. Med. (2015). doi:10.1002/term.1979.

[34] S.J. Roberts, Y. Chen, M. Moesen, J. Schrooten, F.P. Luyten, Enhancement of osteogenic gene expression for the differentiation of human periosteal derived cells, Stem Cell Res. 7 (2011) 137–144. doi:10.1016/j.scr.2011.04.003.

[35] L.F. Freitas Mendes, W.L. Tam, Y.C. Chai, L. Geris, F.P. Luyten, S.J. Roberts, Combinatorial analysis of growth factors reveals the contribution of bone morphogenetic proteins to chondrogenic differentiation of human periosteal cells., Tissue Eng. Part C. Methods. (2016). doi:10.1089/ten.TEC.2015.0436.

[36] J. Bolander, Y.C. Chai, L. Geris, J. Schrooten, D. Lambrechts, S.J. Roberts, F.P. Luyten, Early BMP, Wnt and Ca2+/PKC pathway activation predicts the bone forming capacity of periosteal cells in combination with calcium phosphates, Biomaterials. 86 (2016) 106–118. doi:10.1016/j.biomaterials.2016.01.059.

[37] S.J. Roberts, L. Geris, G. Kerckhofs, E. Desmet, J. Schrooten, F.P. Luyten, The combined bone forming capacity of human periosteal derived cells and calcium phosphates., Biomaterials. 32 (2011) 4393–405. doi:10.1016/j.biomaterials.2011.02.047.

[38] P.B. Ahrens, M. Solursh, R.S. Reiter, Stage-related capacity for limb chondrogenesis in cell culture., Dev. Biol. 60 (1977) 69–82. http://www.ncbi.nlm.nih.gov/pubmed/198274.

[39] K.J. Livak, T.D. Schmittgen, Analysis of relative gene expression data using real-time quantitative PCR and, Methods. 25 (2001) 402–408. doi:10.1006/meth.2001.1262.

[40] U. Galili, The ??-gal epitope and the anti-Gal antibody in xenotransplantation and in cancer immunotherapy, Immunol. Cell Biol. 83 (2005) 674–686. doi:10.1111/j.1440-1711.2005.01366.x.

[41] R.M. Williams, W.R. Zipfel, W.W. Webb, Interpreting second-harmonic generation images of collagen I fibrils., Biophys. J. 88 (2005) 1377–86. doi:10.1529/biophysj.104.047308.

27

[42]   J.M. Menter, Temperature dependence of collagen fluorescence., Photochem. Photobiol. Sci. 5 (2006) 403–10. doi:10.1039/b516429j.

[43]   K. Suhling, L.M. Hirvonen, J.A. Levitt, P.-H. Chung, C. Tregidgo, A. Le Marois, D.A. Rusakov, K. Zheng, S. Ameer-Beg, S. Poland, S. Coelho, R. Henderson, N. Krstajic, Fluorescence lifetime imaging (FLIM): Basic concepts and some recent developments, Med. Photonics. 27 (2015) 3–40. doi:10.1016/j.medpho.2014.12.001.

[44]   T.W. Gilbert, T.L. Sellaro, S.F. Badylak, Decellularization of tissues and organs, Biomaterials. 27 (2006) 3675–3683. doi:10.1016/j.biomaterials.2006.02.014.

[45]   S. Schwarz, L. Koerber, A.F. Elsaesser, E. Goldberg-Bockhorn, A.M. Seitz, L. Dürselen, A. Ignatius, P. Walther, R. Breiter, N. Rotter, Decellularized Cartilage Matrix as a Novel Biomatrix for Cartilage Tissue-Engineering Applications, Tissue Eng. Part A. 18 (2012) 120720085805006. doi:10.1089/ten.tea.2011.0705.

[46]   C.R. Butler, R.E. Hynds, C. Crowley, K.H.C. Gowers, L. Partington, N.J. Hamilton, C. Carvalho, M. Platé, E.R. Samuel, A.J. Burns, L. Urbani, M.A. Birchall, M.W. Lowdell, P. De Coppi, S.M. Janes, Vacuum-assisted decellularization: an accelerated protocol to generate tissue-engineered human tracheal scaffolds., Biomaterials. 124 (2017) 95–105. doi:10.1016/j.biomaterials.2017.02.001.

[47]   A.J. Sutherland, E.C. Beck, S.C. Dennis, G.L. Converse, R.A. Hopkins, C.J. Berkland, M.S. Detamore, Decellularized cartilage may be a chondroinductive material for osteochondral tissue engineering., PLoS One. 10 (2015) e0121966. doi:10.1371/journal.pone.0121966.

[48]   K.E.M. Benders, W. Boot, S.M. Cokelaere, P.R. Van Weeren, D. Gawlitta, H.J. Bergman, D.B.F. Saris, W.J.A. Dhert, J. Malda, Multipotent Stromal Cells Outperform Chondrocytes on Cartilage-Derived Matrix Scaffolds., Cartilage. 5 (2014) 221–30. doi:10.1177/1947603514535245.

[49]   C.C. Rider, Heparin/heparan sulphate binding in the TGF-beta cytokine superfamily., Biochem. Soc. Trans. 34 (2006) 458–60. doi:10.1042/BST0340458.

28

[50]   J. Turnbull, A. Powell, S. Guimond, Heparan sulfate: Decoding a dynamic multifunctional cell regulator, Trends Cell Biol. 11 (2001) 75–82. doi:10.1016/S0962-8924(00)01897-3.

[51]   M.M. French, R.R. Gomes, R. Timpl, M. Höök, K. Czymmek, M.C. Farach-Carson, D.D. Carson, Chondrogenic activity of the heparan sulfate proteoglycan perlecan maps to the N-terminal domain I., J. Bone Miner. Res. 17 (2002) 48–55. doi:10.1359/jbmr.2002.17.1.48.

[52]   G.C. Ingavle, A.W. Frei, S.H. Gehrke, M.S. Detamore, Incorporation of aggrecan in interpenetrating network hydrogels to improve cellular performance for cartilage tissue engineering., Tissue Eng. Part A. 19 (2013) 1349–59. doi:10.1089/ten.TEA.2012.0160.

[53]   N. Mohan, V. Gupta, B. Sridharan, A. Sutherland, M.S. Detamore, The potential of encapsulating "raw materials" in 3D osteochondral gradient scaffolds., Biotechnol. Bioeng. 111 (2014) 829–41. doi:10.1002/bit.25145.

[54]   K. Jochmann, V. Bachvarova, A. Vortkamp, Reprint of: Heparan sulfate as a regulator of endochondral ossification and osteochondroma development, Matrix Biol. 35 (2014) 239–247. doi:10.1016/j.matbio.2014.04.001.

[55]   Y. Lin, H. Lin, Z. Liu, K. Wang, Y. Yan, Improvement of a sample preparation method assisted by sodium deoxycholate for mass-spectrometry-based shotgun membrane proteomics., J. Sep. Sci. 37 (2014) 3321–9. doi:10.1002/jssc.201400569.

[56]   B.D. Elder, D.H. Kim, K.A. Athanasiou, Developing an articular cartilage decellularization process toward facet joint cartilage replacement, Neurosurgery. 66 (2010) 722–727. doi:10.1227/01.NEU.0000367616.49291.9F.

[57]   L. Utomo, M.M. Pleumeekers, L. Nimeskern, S. Nürnberger, K.S. Stok, F. Hildner, G.J.V.M. van Osch, Preparation and characterization of a decellularized cartilage scaffold for ear cartilage reconstruction., Biomed. Mater. 10 (2015) 15010. doi:10.1088/1748-6041/10/1/015010.

29

[58]   S. Nagata, R. Hanayama, K. Kawane, Autoimmunity and the clearance of dead cells., Cell. 140 (2010) 619–30. doi:10.1016/j.cell.2010.02.014.

[59]   M.L. Wong, L.G. Griffiths, Immunogenicity in xenogeneic scaffold generation: antigen removal vs. decellularization., Acta Biomater. 10 (2014) 1806–16. doi:10.1016/j.actbio.2014.01.028.

[60]   S.F. Badylak, T.W. Gilbert, Immune response to biologic scaffold materials, Semin. Immunol. 20 (2008) 109–116. doi:10.1016/j.smim.2007.11.003.

[61]   K.Z. Konakci, B. Bohle, R. Blumer, W. Hoetzenecker, G. Roth, B. Moser, G. Boltz-Nitulescu, M. Gorlitzer, W. Klepetko, E. Wolner, H.J. Ankersmit, Alpha-Gal on bioprostheses: xenograft immune response in cardiac surgery., Eur. J. Clin. Invest. 35 (2005) 17–23. doi:10.1111/j.1365-2362.2005.01441.x.

[62]   A. Mangold, T. Szerafin, K. Hoetzenecker, S. Hacker, M. Lichtenauer, T. Niederpold, S. Nickl, M. Dworschak, R. Blumer, J. Auer, H.J. Ankersmit, Alpha-Gal specific IgG immune response after implantation of bioprostheses., Thorac. Cardiovasc. Surg. 57 (2009) 191–5. doi:10.1055/s-0029-1185395.

[63]   C.S. Park, S.-S. Park, S.Y. Choi, S.H. Yoon, W.-H. Kim, Y.J. Kim, Anti alpha-gal immune response following porcine bioprosthesis implantation in children., J. Heart Valve Dis. 19 (2010) 124–30. http://www.ncbi.nlm.nih.gov/pubmed/20329498.

[64]   F. Gattazzo, A. Urciuolo, P. Bonaldo, Extracellular matrix: a dynamic microenvironment for stem cell niche., Biochim. Biophys. Acta. 1840 (2014) 2506–19. doi:10.1016/j.bbagen.2014.01.010.

[65]   W.A. Horton, M.M. Machado, Extracellular matrix alterations during endochondral ossification in humans., J. Orthop. Res. 6 (1988) 793–803. doi:10.1002/jor.1100060603.

[66]   N. Ortega, D.J. Behonick, Z. Werb, Matrix remodeling during endochondral ossification., Trends Cell Biol. 14 (2004) 86–93. doi:10.1016/j.tcb.2003.12.003.

[67]   J.L. Hyllested, K. Veje, K. Ostergaard, Histochemical studies of the extracellular

30

matrix of human articular cartilage - A review, Osteoarthr. Cartil. 10 (2002) 333–343. doi:10.1053/joca.2002.0519.

[68]   N. Schmitz, S. Laverty, V.B. Kraus, T. Aigner, Basic methods in histopathology of joint tissues, Osteoarthr. Cartil. 18 (2010). doi:10.1016/j.joca.2010.05.026.

[69]   P. Than, Differential scanning calorimetric examination of the osteoarthritic hyaline cartilage in rabbits, Thermochim. Acta. 404 (2003) 149–153. doi:10.1016/S0040-6031(03)00146-1.

[70]   C.B. Talbot, M.J. Lever, R.K.P. Benninger, J. Mcginty, J. Requejo-Isidro, D.S. Elson, P.M.W. French, A. Sandison, A.L. Wallace, H. Nagase, Y. Itoh, J. Saklatvala, T. Vincent, Fluorescence lifetime imaging of articular cartilage, Int. J. Exp. Pathol. 85 (2008) A31–A32. doi:10.1111/j.0959-9673.2004.369ao.x.

[71]   H. Akkiraju, A. Nohe, Role of Chondrocytes in Cartilage Formation, Progression of Osteoarthritis and Cartilage Regeneration., J. Dev. Biol. 3 (2015) 177–192. doi:10.3390/jdb3040177.

[72]   M.M.J. Caron, P.J. Emans, M.M.E. Coolsen, L. Voss, D.A.M. Surtel, A. Cremers, L.W. van Rhijn, T.J.M. Welting, Redifferentiation of dedifferentiated human articular chondrocytes: comparison of 2D and 3D cultures., Osteoarthr. Cartil. 20 (2012) 1170–8. doi:10.1016/j.joca.2012.06.016.

[73]   S.R. Tew, P. Pothacharoen, T. Katopodi, T.E. Hardingham, SOX9 transduction increases chondroitin sulfate synthesis in cultured human articular chondrocytes without altering glycosyltransferase and sulfotransferase transcription., Biochem. J. 414 (2008) 231–6. doi:10.1042/BJ20080262.

[74]   J. Chen, Y. Wang, C. Chen, C. Lian, T. Zhou, B. Gao, Z. Wu, C. Xu, Exogenous Heparan Sulfate Enhances the TGF-β3-Induced Chondrogenesis in Human Mesenchymal Stem Cells by Activating TGF-β/Smad Signaling., Stem Cells Int. 2016 (2016) 1520136. doi:10.1155/2016/1520136.

[75]   S.-H. Kim, J. Turnbull, S. Guimond, Extracellular matrix and cell signalling: the

31

dynamic cooperation of integrin, proteoglycan and growth factor receptor., J. Endocrinol. 209 (2011) 139–51. doi:10.1530/JOE-10-0377.

[76]   P.M. Van der Kraan, P. Buma, T. Van Kuppevelt, W.B. Van Den Berg, Interaction of chondrocytes, extracellular matrix and growth factors: Relevance for articular cartilage tissue engineering, Osteoarthr. Cartil. 10 (2002) 631–637. doi:10.1053/joca.2002.0806.

[77]   K. Oka, S. Oka, T. Sasaki, Y. Ito, P. Bringas, K. Nonaka, Y. Chai, The role of TGF-beta signaling in regulating chondrogenesis and osteogenesis during mandibular development., Dev. Biol. 303 (2007) 391–404. doi:10.1016/j.ydbio.2006.11.025.

[78]   M.K. Murphy, D.J. Huey, J.C. Hu, K.A. Athanasiou, TGF-β1, GDF-5, and BMP-2 stimulation induces chondrogenesis in expanded human articular chondrocytes and marrow-derived stromal cells., Stem Cells. 33 (2015) 762–73. doi:10.1002/stem.1890.

[79]   M.B. Ellman, H.S. An, P. Muddasani, H.-J. Im, Biological impact of the fibroblast growth factor family on articular cartilage and intervertebral disc homeostasis., Gene. 420 (2008) 82–9. doi:10.1016/j.gene.2008.04.019.

[80]   C. Colnot, Skeletal cell fate decisions within periosteum and bone marrow during bone regeneration., J. Bone Miner. Res. 24 (2009) 274–82. doi:10.1359/jbmr.081003.

[81]   X. Zhang, C. Xie, A.S.P. Lin, H. Ito, H. Awad, J.R. Lieberman, P.T. Rubery, E.M. Schwarz, R.J. O'Keefe, R.E. Guldberg, Periosteal progenitor cell fate in segmental cortical bone graft transplantations: implications for functional tissue engineering., J. Bone Miner. Res. 20 (2005) 2124–37. doi:10.1359/JBMR.050806.

[82]   S.J. Roberts, N. van Gastel, G. Carmeliet, F.P. Luyten, Uncovering the periosteum for skeletal regeneration: The stem cell that lies beneath, Bone. 70 (2015) 10–18. doi:10.1016/j.bone.2014.08.007.

[83]   Z. Lin, A. Fateh, D.M. Salem, G. Intini, Periosteum: biology and applications in

32

craniofacial bone regeneration., J. Dent. Res. 93 (2014) 109–16.
doi:10.1177/0022034513506445.

[84]   Q. Zheng, G. Zhou, R. Morello, Y. Chen, X. Garcia-Rojas, B. Lee, Type X collagen gene
regulation by Runx2 contributes directly to its hypertrophic chondrocyte-specific
expression in vivo., J. Cell Biol. 162 (2003) 833–42. doi:10.1083/jcb.200211089.

[85]   F. Li, Y. Lu, M. Ding, D. Napierala, S. Abbassi, Y. Chen, X. Duan, S. Wang, B. Lee, Q.
Zheng, Runx2 contributes to murine Col10a1 gene regulation through direct
interaction with its cis-enhancer., J. Bone Miner. Res. 26 (2011) 2899–910.
doi:10.1002/jbmr.504.

[86]   B.N. Brown, J.E. Valentin, A.M. Stewart-Akers, G.P. McCabe, S.F. Badylak,
Macrophage phenotype and remodeling outcomes in response to biologic scaffolds
with and without a cellular component., Biomaterials. 30 (2009) 1482–91.
doi:10.1016/j.biomaterials.2008.11.040.

[87]   B.R. Olsen, A.M. Reginato, W. Wang, Bone development., Annu. Rev. Cell Dev. Biol.
16 (2000) 191–220. doi:10.1146/annurev.cellbio.16.1.191.

[88]   P. Klinger, C. Surmann-Schmitt, M. Brem, B. Swoboda, J.H. Distler, H.D. Carl, K. Von
Der Mark, F.F. Hennig, K. Gelse, Chondromodulin 1 stabilizes the chondrocyte
phenotype and inhibits endochondral ossification of porcine cartilage repair tissue,
Arthritis Rheum. 63 (2011) 2721–2731. doi:10.1002/art.30335.

[89]   C. Scotti, B. Tonnarelli, A. Papadimitropoulos, A. Scherberich, S. Schaeren, A.
Schauerte, J. Lopez-Rios, R. Zeller, A. Barbero, I. Martin, Recapitulation of
endochondral bone formation using human adult mesenchymal stem cells as a
paradigm for developmental engineering., Proc. Natl. Acad. Sci. U. S. A. 107 (2010)
7251–6. doi:10.1073/pnas.1000302107.

[90]   R. Osinga, N. Di Maggio, A. Todorov, N. Allafi, A. Barbero, F. Laurent, D.J. Schaefer, I.
Martin, A. Scherberich, Generation of a Bone Organ by Human Adipose-Derived
Stromal Cells Through Endochondral Ossification., Stem Cells Transl. Med. 5 (2016)
1090–7. doi:10.5966/sctm.2015-0256.

33

[91] C. Scotti, E. Piccinini, H. Takizawa, A. Todorov, P. Bourgine, A. Papadimitropoulos, A. Barbero, M.G. Manz, I. Martin, Engineering of a functional bone organ through endochondral ossification., Proc. Natl. Acad. Sci. U. S. A. 110 (2013) 3997–4002. doi:10.1073/pnas.1220108110.

34
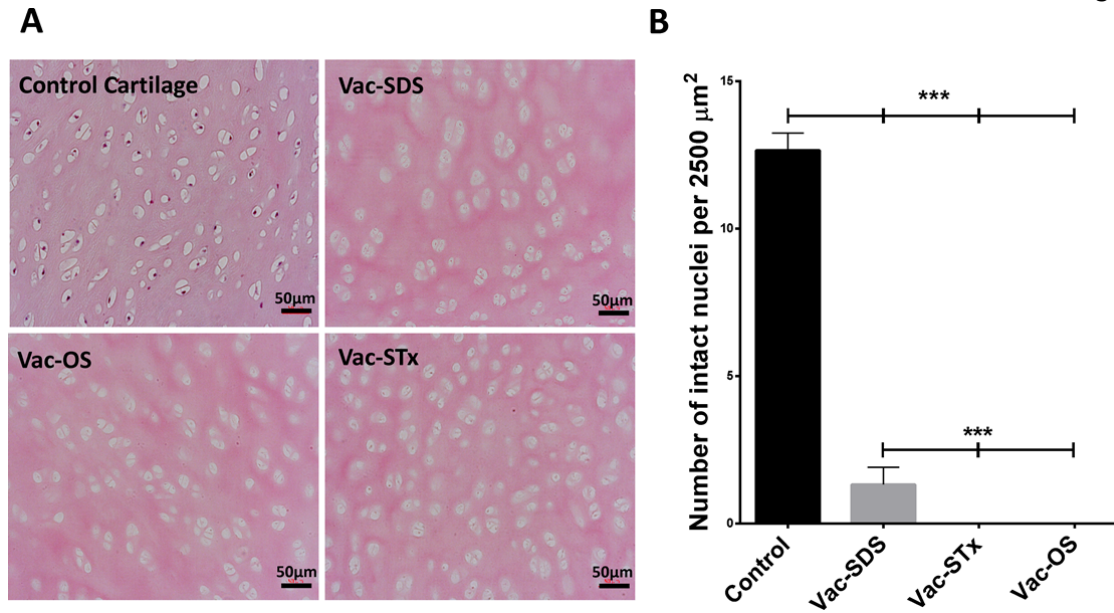
Figure 1: Vac-OS and Vac-STx based decellularisation methodologies result in complete clearance of intact cellular nuclei. (A) Representative histological (n=3) analysis of cellular clearance from hyaline cartilage indicates removal of cellular content (scale bar = 50 μm). (B) Image-based quantification of intact nuclei using ImageJ presented as mean ±SD (n=3 **p<0.01, ***p<0.001). Statistical analysis performed using a one-way ANOVA using Bonferroni's posthoc correction.
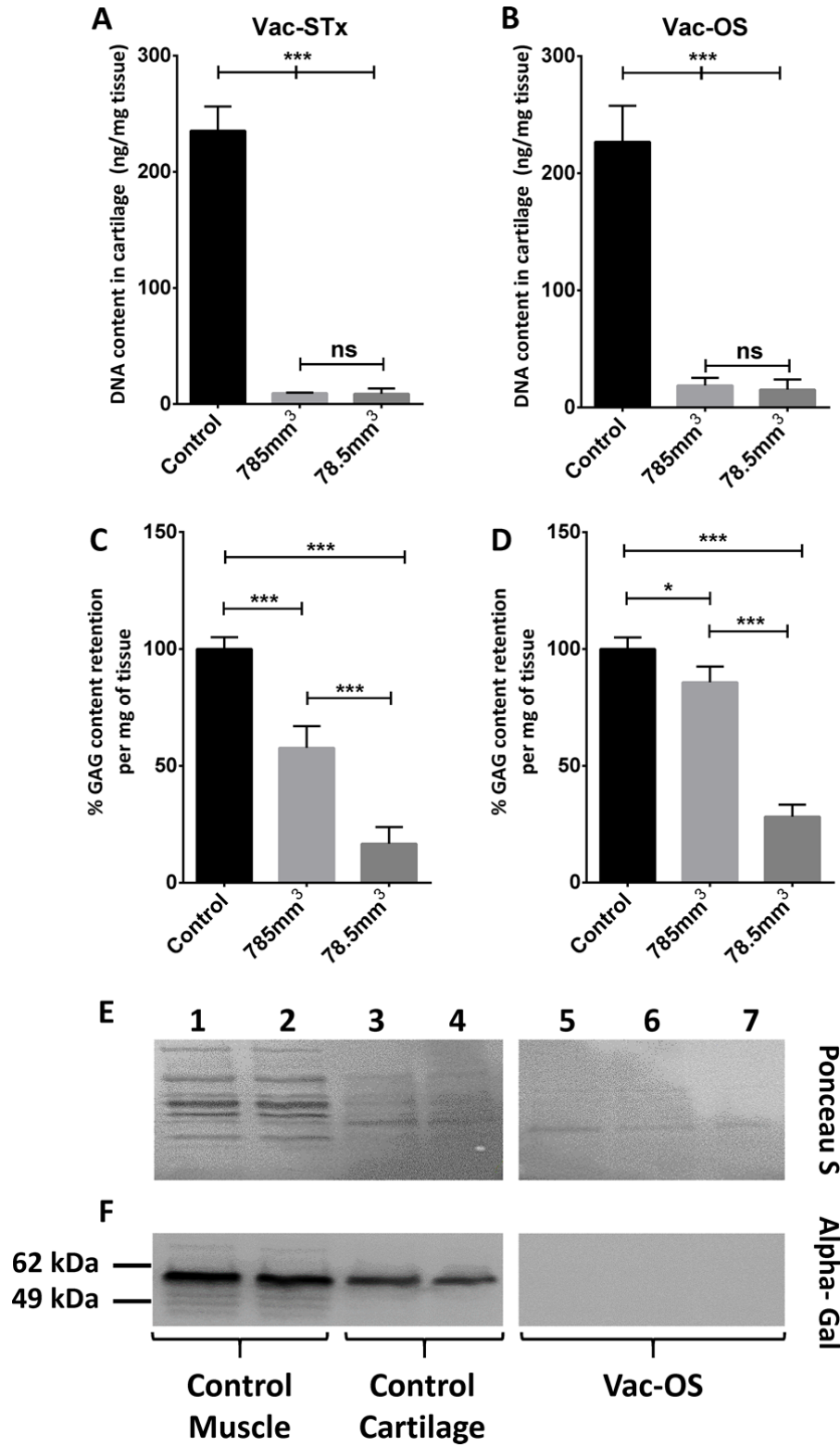
Figure 2: Upscaling scaffold size does not impede DNA clearance but does enhance GAG retention. DNA content in cartilage subjected to (A) Vac-STx (n=3) and (B) Vac-OS (n=5)

36

based methodologies. Data presented as mean ng/mg wet mass of tissue ±SD. Both scaffold volume DNA contents fell below the threshold of 50 ng/mg for the Vac-STx and Vac-OS treated samples. Percentage sGAG content per mg wet mass tissue ±SD, subjected to (C) Vac-STx (n=3) and (D) Vac-STx (n=5) methodologies, normalised to native cartilage sGAG content. Statistical analysis was performed using a one-way ANOVA, using Bonferonni's posthoc correction. Vac-OS decellularisation eliminates highly immunogenic alpha-Gal epitopes. (E) Representative images of Ponceau S staining of transferred proteins indicating the presence of protein bands in each lane. (F) Representative Immunoblot image illustrating the presence of the Alpha-Gal epitope at 56 kDa in both the control muscle (lanes 1&2), control cartilage samples (lanes 3 &4) and absence in Vac-OS decellularised cartilage (lanes 5, 6 &7) (n=3).

37
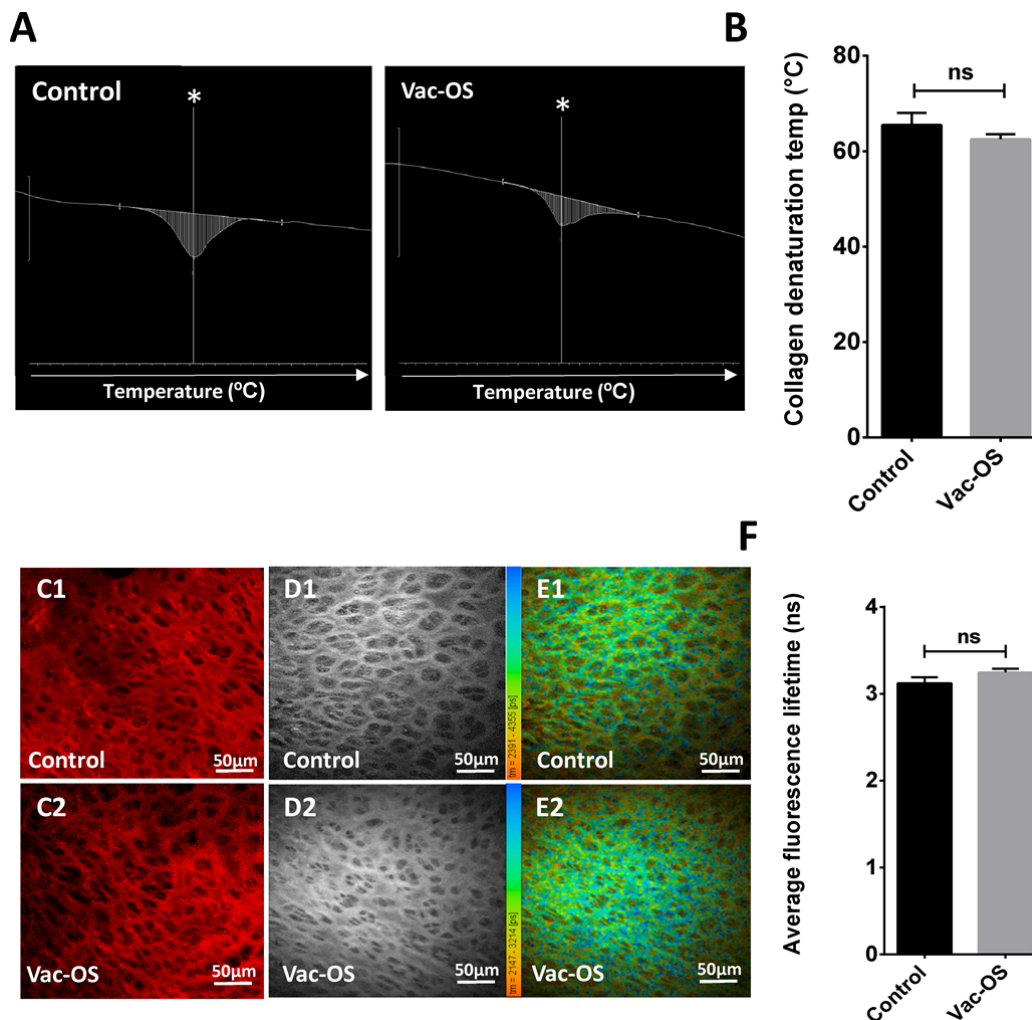
Figure 3: Vac-OS decellularised ECM matrix integrity is maintained post decellularisation.
Example differential scanning calorimetry thermal analysis curves and quantification of average denaturation temperatures comparing control cartilage vs dcECM samples, (*Peak denaturation temperature). (C) Second harmonic generation (SHG) microscopy image. The dcECM (C2) retains its architecture with minimal changes observed in lacunae size. (D) Two-photon autofluorescence image at 720 nm excitation. (E) False coloured fluorescence lifetime imaging microscopy (FLIM) images indicative of the distribution of the fluorescence lifetimes of the samples. (F) ImageJ quantification of the ROI's, measuring the average fluorescence lifetimes (n=3). Representative quantification data are represented as mean ± SD. Statistical analysis performed using an unpaired t-test with Welch's posthoc correction.

38
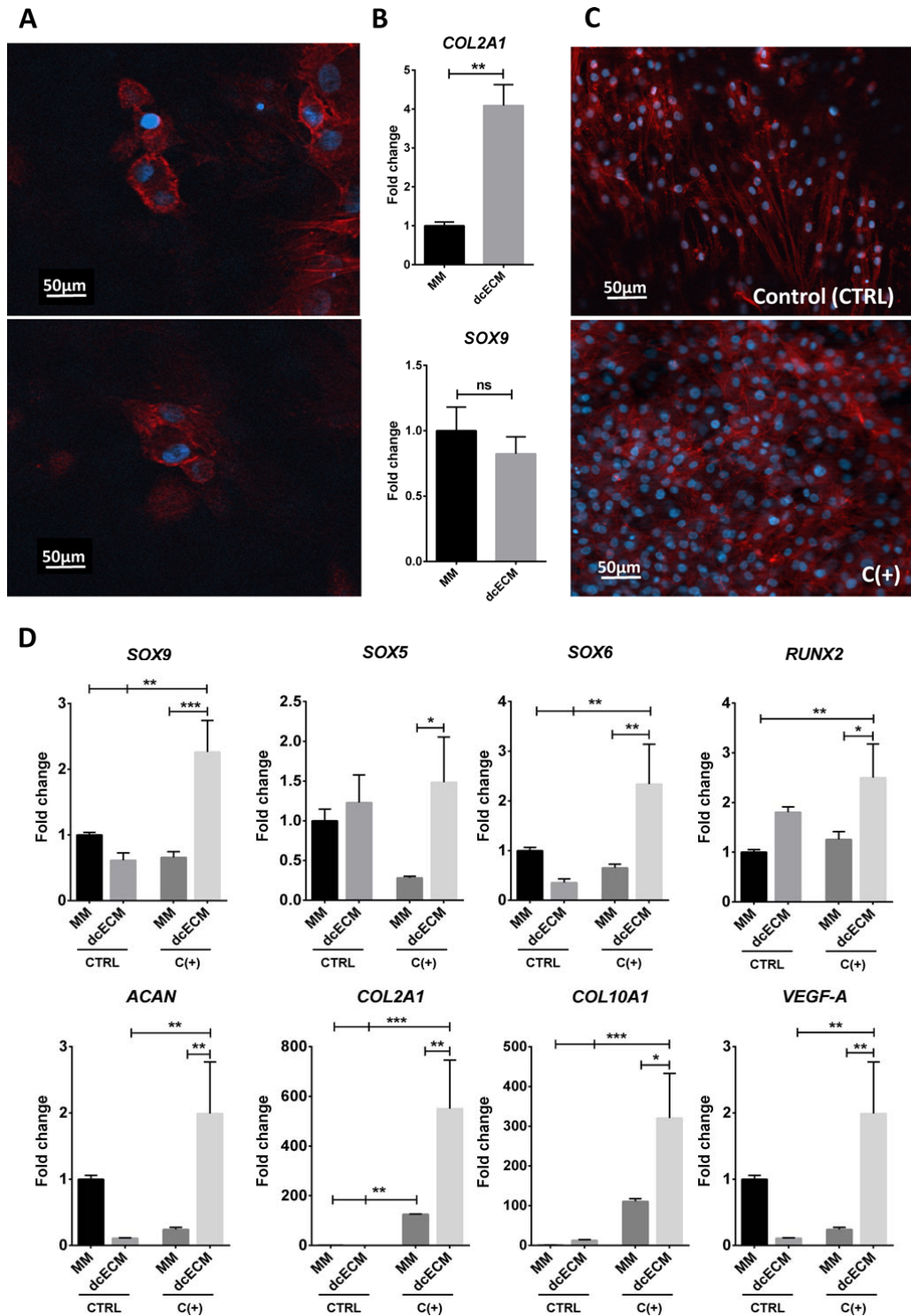
Figure 4: dcECM promotes cell attachment and upregulates chondrogenic gene expression of skeletal cell populations. (A) Structured illumination microscopy images of dedifferentiated chondrocytes seeded on dcECM and stained with DAPI/phalloidin

39

indicating cells residing within the lacunae. (B) Chondrogenic markers; *SOX9* and *COL2A1* mRNA expression as measured by qPCR. Results are expressed as the mean fold change normalised to micromass (MM) culture conditions ± SD (n=3 **$p<0.01$). Statistical analysis performed using a unpaired t-test with Welch's posthoc correction. (C) Representative fluorescence images of hPDSCs seeded in micromass and on the dcECM under control conditions [CTRL] and chondrogenic conditions [C(+)] containing TGF-β. Fluorescence images were obtained using structured illumination (scale bar = 50 µm). (D) Chondrogenic gene expression of hPDSCs seeded in MM and dcECM under control conditions (CTRL) and C(+) conditions. *SOX9, SOX5, SOX6, ACAN, COL2A1, VEGF-A, COL10A1* and *RUNX2* mRNA expression were measured by qPCR. Results are expressed as the mean fold change normalised to micromass cultures in control (MM-CONTROL) conditions ± SD (n=3 *$p<0.05$, **$p<0.01$, ***$p<0.001$).   Statistical analysis was performed using one-way ANOVA corrected for multiple comparisons using Bonferroni's posthoc analysis.

40
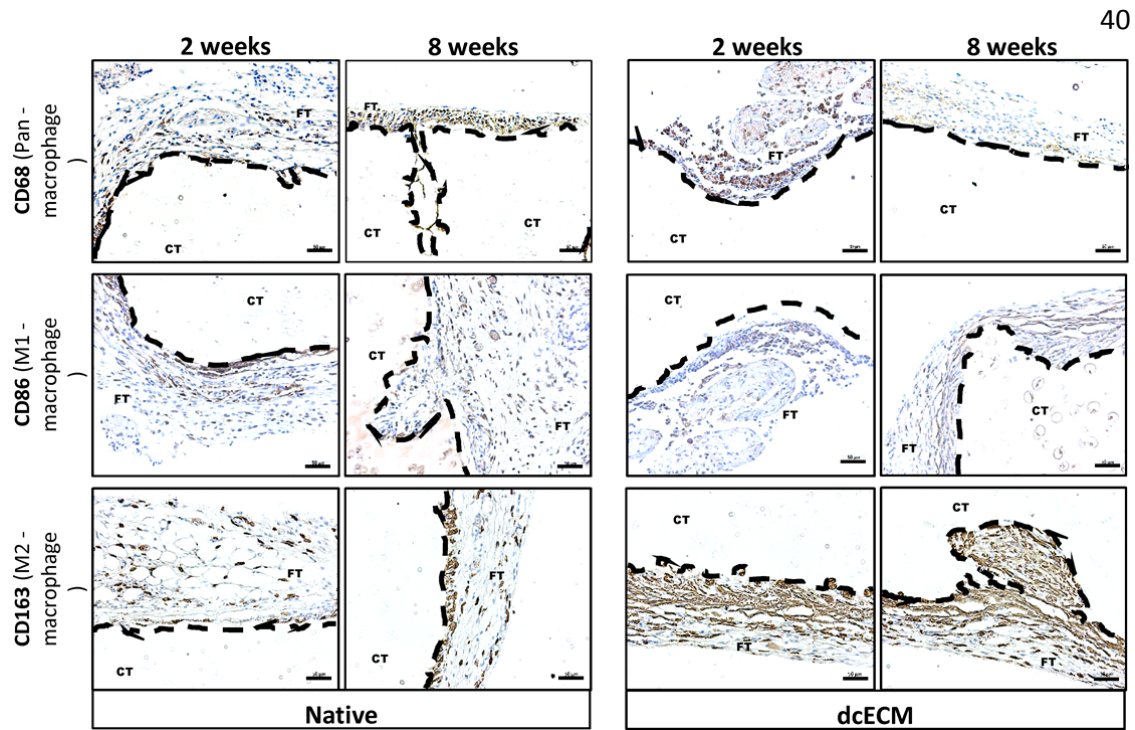
Figure 5: dcECM implanted into immunocompetent mice results in a predominantly M2 macrophage-mediated response. Representative brightfield images of subcutaneously implanted native and dcECM cartilaginous constructs (CT) and host cellular infiltrate (FT). IHC was performed to visualise CD68 (Pan-macrophage marker), CD86 (M1-macrophage marker) and CD163 (M2-macrophage marker). Scale bars = 50 µm.

41

Supplementary Table 1: Decellularisation methodologies, highlighting each step along with the length of time

Vac-OS	Vac-STx	Vac-SDS
Freeze/Thaw Length: 24 Hours	**Freeze/Thaw** Length: 24 Hours	**Freeze/Thaw** Length: 24 Hours
Distilled Water Length: 6 Hours	**0.25% Triton X + 0.25% SOC** Length: 24 Hours	**1% SDS** Length: 4 Hours
Hypertonic Solution Length: 12 Hours	**HBSS** Length: 24 Hours	**PBS** Length: 12 Hours
Wash Buffer Length: 12 Hours	**DNAse/RNAse** Length: 24 Hours	**Hypertonic Sol** Length: 10 Hours
Hypotonic Solution Length: 12 Hours	**HBSS** Length: 24 Hours	**PBS** Length: 12 Hours
DNAse/RNAse Length: 24 Hours	Sterilisation	**Hypotonic Sol** Length: 10 Hours
Wash Buffer Length: 12 Hours		**DNAse/RNAse** Length: 12 Hours
PBS Length: 12 Hours		**PBS** Length: 24 Hours
Sterilisation		Sterilisation

Supplementary Table 2: Primer sequences used in the study

Gene ID	NCBI accession number		Sequence 5'-3'
COL2A1	NM_001844.4	Forward	GGCTTCCATTTCAGCTATGG
		Reverse	AGCTGCTTCGTCCAGATAGG
SOX9	NM_000346.3	Forward	TGGAGACTTCTGAACGAGAGC
		Reverse	CGTTCTTCACCGACTTCCTC
SOX5	NM_001261414.2	Forward	TGCTTACTGACCCTGATTTACC
		Reverse	CACTCTCCTCTTCTTCCACTTTC
SOX6	NM_001145811.1	Forward	AACAACGGCAGCAAATGGAC
		Reverse	CATGTGACCCTGAACCTGGA
VEGF-A	NM_001025366.2	Forward	AGTCCAACATCACCATGCAG
		Reverse	TTCCCTTTCCTCGAACTGATTT
RUNX2	NM_001015051.3	Forward	CGCATTCCTCATCCCAGTAT
		Reverse	GCCTGGGGTCTGTAATCTGA
COL10A1	NM_000493.3	Forward	ACGATACCAAATGCCCACAG
		Reverse	GTGGACCAGGAGTACCTTGC
ACAN	NM_001135.3	Forward	TGTGGGACTGAAGTTCTTGG
		Reverse	AGCGAGTTGTCATGGTCTG
HPRT1	NM_000194.2	Forward	TGAGGATTTGGAAAGGGTGT
		Reverse	GAGCACACAGAGGGCTACAA

43
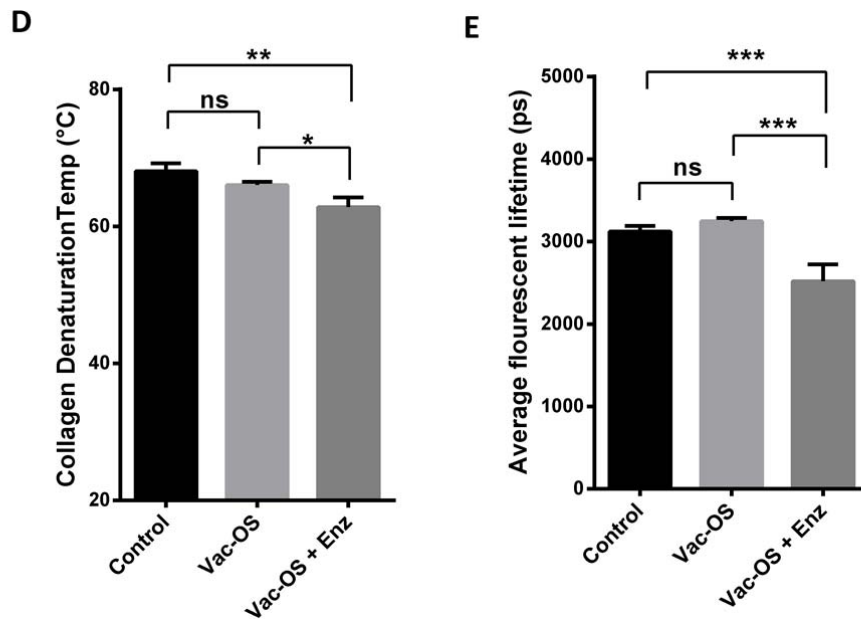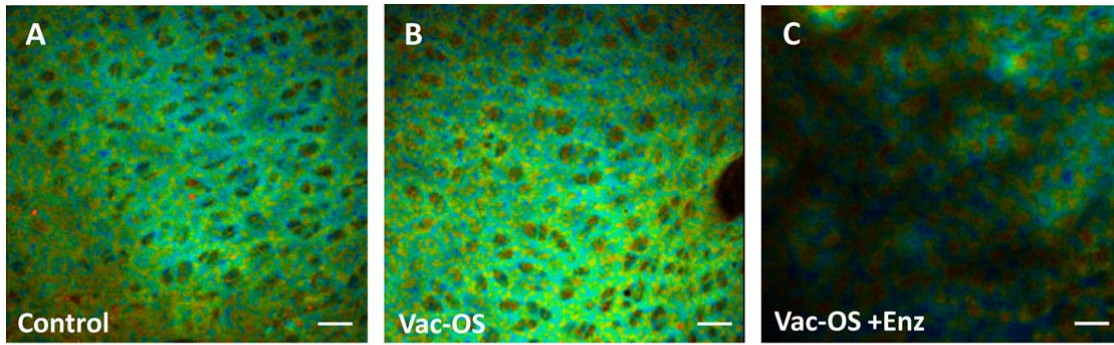
Supplementary figure 1: Further disruption of the Vac-OS decellularised scaffold using collagenase results in significant collagen denaturation and fluorescence changes. (A-C) False coloured fluorescence lifetime imaging microscopy (FLIM) images indicative of the distribution of the fluorescence lifetimes within the samples. (D) Quantification of average denaturation temperatures comparing control cartilage vs dcECM vs collagenase treated Vac-OS samples. (E) ImageJ quantification of the ROI's, measuring the average fluorescence lifetimes (n=3). Representative quantification data is represented as mean ± SD. Statistical analysis performed using a unpaired t-test with Welch's post-hoc correction.